Seventh International Conference on Computational Fluid Dynamics (ICCFD7), Big Island, Hawaii, July 9-13, 2012

ICCFD7-4503

CFD Simulations of the Wind Environment at Shonai Airport Integrated with Weather Prediction Data

K. Shimoyama*, H. Nakanomyo* and S. Obayashi*
Corresponding author: obayashi@ifs.tohoku.ac.jp

* Institute of Fluid Science, Tohoku University, Japan.

Abstract: Wind environment at an airport is affected by geographic features. In Japan, Shonai Airport is known to have wind shear over the runway due to the turbulence induced by the neighboring hill frequently in winter. This study performed large eddy simulation (LES) to investigate the turbulence around Shonai Airport. The initial and boundary conditions were given according to the weather prediction data by the Japan Meteorological Agency non-hydrostatic model (JMANHM). These data were downscaled and transferred to LES domains, which considered actual geographical features as the boundary conditions on the ground, using the two-way nesting method. The present simulations indicated that geographical features may have an significant influence on the turbulence appearing in flight path, i.e., aircraft safety depending on wind direction. In addition, it was also indicated that the present simulation can predict the turbulence induced by geographical features, and agree with the turbulence, which was actually observed by the Doppler radar.

Keywords: LES, Weather Prediction, Wind, Airport.

1 Introduction

Wind environment around an airport is affected by various causes, such as wake turbulence and wind turbulence caused by meteorological and geographical features. These turbulence problems are major hazards to airport traffic management.

Wake turbulence is generated behind a flying airplane. Especially, it becomes strong in takeoff and landing conditions where high lift is required. Therefore, airport traffic management provides a certain separation for departure and arrival to maintain the safety of a following aircraft. On the other hand, the demand for air traffic is expected to increase in coming decades, therefore airport operation should be more efficient. It is most desirable to increase the number of takeoffs and landings by shortening the separation between aircrafts without sacrificing the safety of a following aircraft.

For this purpose, our research group has been working on understanding the behaviors of wake turbulence in Sendai Airport, Japan, which is nearest to our university. The study in [1] measured the wake turbulence, which appeared just after an aircraft took off from the runway, by light detection and ranging (LIDAR), which can detects the line-of-sight velocity component of aerosol in the air based on the Doppler shift. In addition, the study in [2] simulated the wake turbulence by integrating the LIDAR measurement data with computational fluid dynamics (CFD) simulation using a four-dimensional variational data assimilation method (a.k.a. adjoint method). In that simulation, the initial and boundary conditions are adjusted so that the solution obtained by simulation will coincide with real-world measurement. However, LIDAR measurement is still limited to be available in several airports, so the study in [3] conducted the CFD simulation of wake turbulence integrated with weather prediction data. That simulation employed a nesting method to bridge the gap of scale between wake turbulence and weather features (horizontal roll convection currents in sea breeze).

Airport wind environment is also affected by the geographical features. For example, in Japan, the study in [4] reported that LIDAR measurement revealed the turbulence caused by a hanger of aircrafts in

Haneda International Airport. There are other reports in [5, 6] that Shonai Airport decreases the in-service rate in winter seasons due to low-level wind turbulence, which is caused by the interference of a strong seasonal wind (monsoon) with a hill in the neighborhood of the airport. To date, in Shonai Airport, Japan aerospace exploration agency (JAXA) has conducted measurements of wind turbulence using Doppler radar and LIDAR. However, those measurements still have lack in coverage and accuracy especially to detect low-level head wind. Therefore, it is expected to investigate the mechanisms of geography-induced turbulence by CFD simulation with higher resolution than the measurements. However, there is no precedent simulation for this phenomenon.

In this study, large eddy simulation (LES) around Shonai Airport was performed by using the two-way nesting method. In this simulation, detailed geographical feature data are placed in the simulation domain to simulate the turbulence induced by the neighboring hill. First, turbulence simulations were performed with uniform background flow conditions. Next, the turbulence simulation was integrated with the weather prediction data on the date when the turbulence was actually observed by the Doppler radar. Thus, this study validated the consistency of the present simulation with a real-world turbulence phenomenon.

2 Simulation Case

Shonai Airport is located near the west coast of north-eastern Japan, as shown in Fig. 1. This airport is known to have wind shear over the flight path frequently in winter due to the turbulence of the neighboring hill, which is located in the north of the airport. As the simulation case, this study considered the time range from 07:30 to 08:30 on February 6, 2010 (in Japan standard time), when turbulence was actually observed by the Doppler radar located beside the end of runway (RWY27); the wind speeds reached 26kt (13.4m/s) on average and 41kt (21.1m/s) at maximum.

Figure 1: Location of Shonai Airport.

3 Numerical Methodologies

The present simulation employed the two-way nesting method to integrate LES with weather prediction, each of which was simulated using different governing equations and models in a different zone with different scales. Figure 2 shows the simulation domain and the flowchart considered in the two-way nesting method [7].

3.1 Weather Prediction

Weather prediction was conducted in the largest zone (denoted as "JMANHM (Δ50m)" in Fig. 2(a)), which has the size of 3450m $\times$ 3200m $\times$ 500m in the east-west (x), north-south (y), and vertical (z) directions, respectively. The mesh points are allocated at every 50m in x and y directions evenly and at $z = 10\text{m}, 30\text{m}, 52\text{m}, 75\text{m}, \cdots$ (every 25m) $\cdots$, 500m locations in z direction.

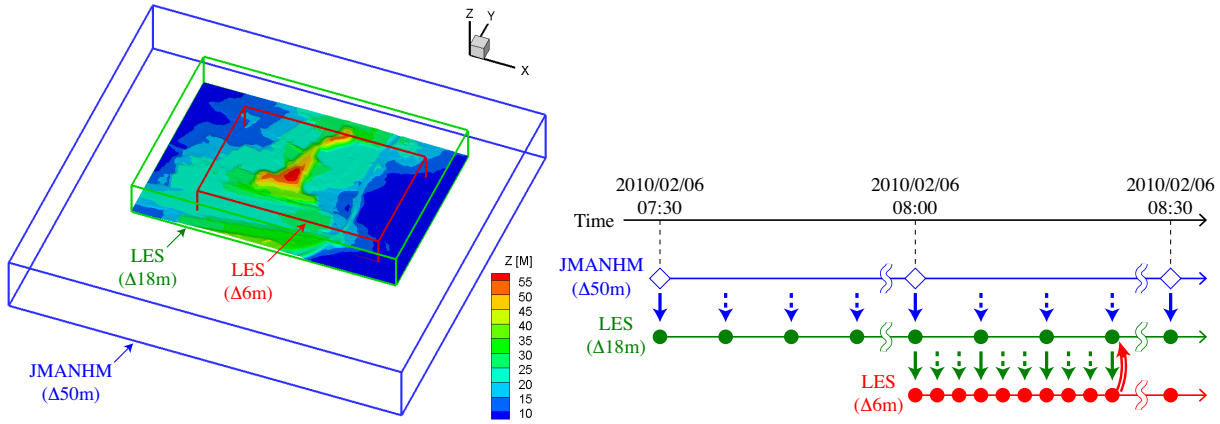

(a) Simulation Domain (b) Flowchart

Figure 2: Two-Way Nesting Method.

This study employed the Japan Meteorological Agency non-hydrostatic model (JMANHM) [8]; it solved the fully compressible atmospheric equations with the Lambert conformal projection and obtained momentum, perturbation pressure, and potential temperature as the prognostic variables using the horizontally implicit-vertical implicit (HI-VI) time integration scheme. Some physical processes, such as land surface process, boundary layer turbulence process, and cloud microphysical process were also implemented in JMANHM. The initial conditions were given at 00:00 on February 6, 2010 by the mesoscale model (MSM) of the Japan Meteorological Agency. The boundary conditions on the ground were given by the global 30 arc second elevation data set (GTOPO30) [9] and the global land cover characterization (GLCC) database [10] provided by the United States Geological Survey.

Figure 3 shows the plots of wind velocity at three sequential times (07:30, 08:00, and 08:30 on February 6, 2010), which were predicted by JMANHM. Northwesterly winds seem dominant in these plots and have the speeds of 13.4m/s on average and 16.1m/s at maximum, which agree with the actual wind direction and speeds observed by the Doppler radar. Therefore, this study considered these data to be valid for the following turbulence simulations.

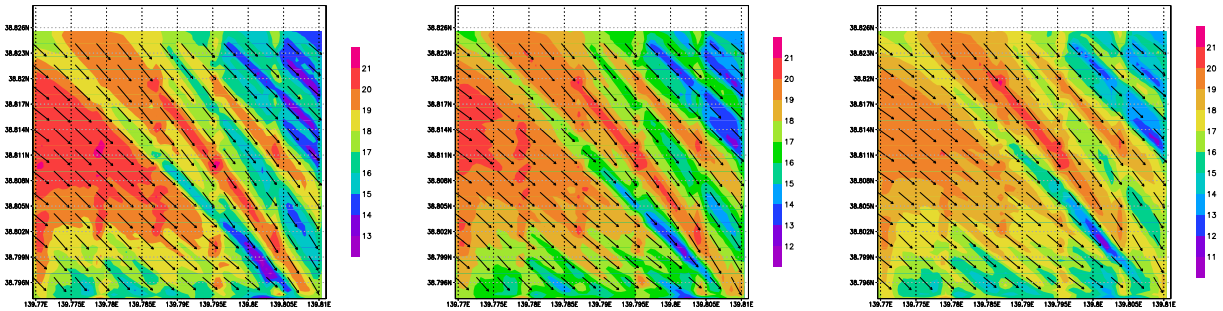

(a) 2010/02/06 07:30 (b) 2010/02/06 08:00 (c) 2010/02/06 08:30

Figure 3: Plots of Wind Velocity Predicted by JMANHM (Contour: Velocity Magnitude [m/s], Vector: Velocity Direction).

3.2 Large Eddy Simulation

LES of turbulence was conducted in two smaller zones (denoted as "LES (Δ18m)" and "LES (Δ6m)" in Fig. 2(a)). The former zone has the size of 2340m × 1620m × 306m in x, y, and z directions, respectively, and the mesh points are allocated at every 18m in all the directions evenly. The latter has the size of 1590m × 1050m × 246m in x, y, and z directions, respectively, and the mesh points are allocated at every 6m

in all the directions evanly. These zones contain geographical data, which are represented by the staircase mesh shown in Fig. 4, based on the digital elevation model [11] provided by the Geospatial Information Authority of Japan.

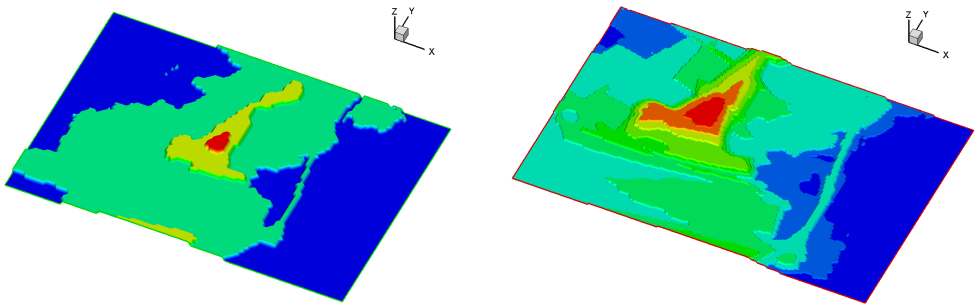

(a) LES (Δ18m) (b) LES (Δ6m)

Figure 4: Geographical Data.

The present LES solved the Favre-filtered Navier-Stokes equations for compressible air, in which the subgrid-scale turbulence was modeled by the Smagorinsky model with Shen's special treatment to suppress immoderate production of eddy viscosity at vortex centers [12]. The convective terms were evaluated by Roe's upwind flux difference splitting (FDS) scheme [13], in which fourth-order accuracy was obtained by the monotone upstream-centered schemes for conservation laws (MUSCL) [14] based on the primitive variables without flux limiters. The viscous terms were evaluated by the second-order central differencing. Time integration of the Navier-Stokes equations was performed by the fourth-order Runge-Kutta method.

The initial and boundary conditions were characterized by the two-way nesting method as follows (also see Fig. 2(b)). LES (Δ18m) zone referred to the weather prediction data in JMANHM (Δ50m) zone as the initial conditions and the boundary conditions at each time step. Note that the weather prediction data were given at limited locations and times (07:30, 08:00, and 08:30 on February 6, 2010), and linearly interpolated in space and time so as to estimate the weather at any location and time. After LES (Δ18m) zone run the simulation from 07:30 to 08:00, LES (Δ6m) zone started the simulation from 08:00. LES (Δ6m) zone received coarser flow solutions from LES (Δ18m) zone through linear interpolation, and employed them as the initial conditions and the boundary conditions at each time step. Time step size in LES (Δ6m) zone was set to be 1/3 of that in LES (Δ18m) zone to keep a same Courant number. On the other hand, LES (Δ18m) zone received finer flow solutions from LES (Δ6m) zone at every nine time steps, and replaced the coarser solutions with the finer solutions at the mesh points overlapping between these zones.

4 Results and Discussions

First, turbulence simulations around Shonai Airport were performed under uniform background wind conditions with different directions to investigate the effects of the neighboring hill on the turbulence. Next, the turbulence simulation was integrated with weather prediction data and validated through a comparison with the actual measurement data, which detected the turbulence by the Doppler radar on February 6, 2010.

4.1 Under Uniform Background Wind Conditions

In this section, turbulence simulations were conducted by assuming uniform background wind with a constant speed of 13.4m/s (averaged wind speed in the actual measurement by the Doppler radar) as the initial and boundary conditions in LES (Δ18m), while the weather prediction data given in JMANHM (Δ50m) zone were not transferred to the LES zones. In addition, the direction of uniform background wind was set to be 0deg, 30deg, and 60deg for parametric study.

Figure 5 shows the isosurface plots of the vertical (z) component of wind velocity under uniform background wind conditions. The isosurfaces reveal the structures of turbulence, which is caused in the downstream of the hill when the wind goes around it. These structures move across the RWY27 flight path and

seem to influence the safety of landing aircrafts when the wind directions are 30deg and 60deg. On the other hand, such influences seem not to be significant when the wind direction is 0deg and almost parallel to the runway.

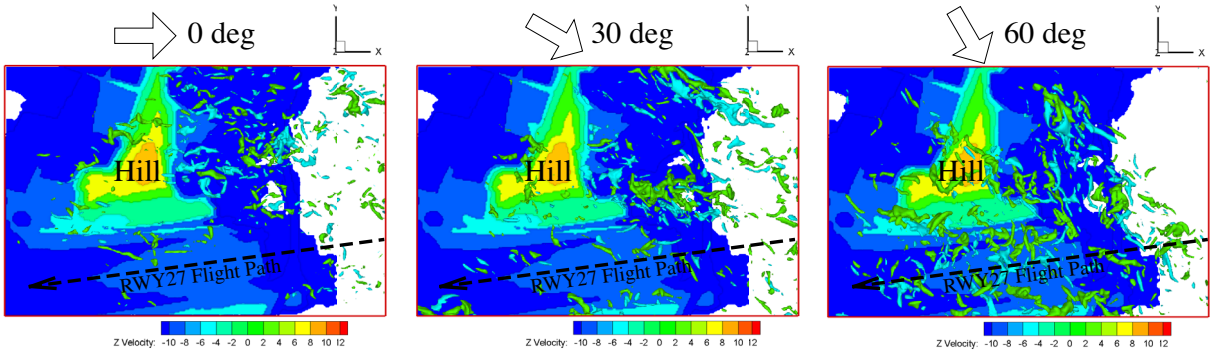

(a) Wind Direction = 0deg (b) Wind Direction = 30deg (c) Wind Direction = 60deg

Figure 5: Isosurface Plots of the Vertical Component of Wind Velocity [m/s] Under Uniform Background Wind Conditions.

Figure 6 shows the profiles of wind velocity magnitude along the flight path under uniform background wind conditions. These profiles contain the averaged values for 30s as solid lines and the maximum and minimum values as error bars. The flight path, shown as a broken line, assumes to have a descent angle of 3deg. Compared to the case with the wind direction of 0deg, the cases with the wind direction of 30deg and 60deg involve smaller averages and larger variations of wind velocity magnitude in almost the whole flight path ($0\text{m} \leq x \leq 900\text{m}$). This is because the flight path is included in the unsteady wake flow behind the hill. Therefore, the results in this section indicate that geographical features may have an significant influence on the turbulence appearing in flight path, i.e., aircraft safety depending on wind direction.

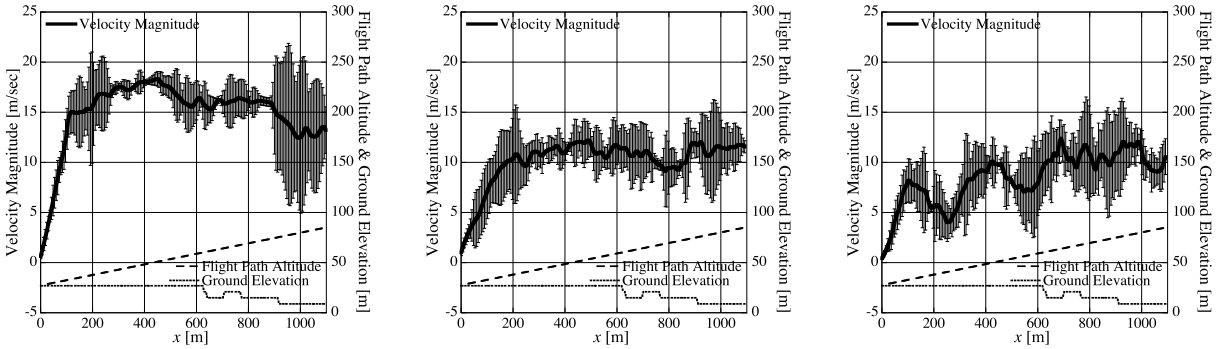

(a) Wind Direction = 0deg (b) Wind Direction = 30deg (c) Wind Direction = 60deg

Figure 6: Profiles of Wind Velocity Magnitude Along Flight Path Under Uniform Background Wind Conditions.

4.2 Under the Conditions Integrated with Weather Prediction Data

In this section, the turbulence simulation was conducted by downscaling and transferring the weather prediction data given in JMANHM (Δ50m) to the LES zones as real-world environments with non-uniform unsteady background wind conditions.

Figure 7 shows the isosurface plot of the vertical (z) component of wind velocity, which reveals the structures of turbulence caused by the hill, under the conditions integrated with the weather prediction data. These structures move across the flight path due to the northwesterly winds as seen in Fig. 3.

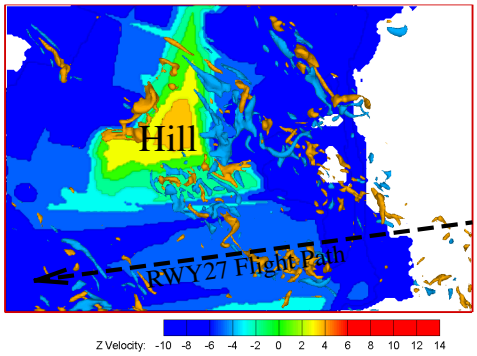

Figure 7: Isosurface Plot of the Vertical Component of Wind Velocity [m/s] Under the Conditions Integrated with Weather Prediction Data.

Figure 8 shows the vertical (z) profiles of wind velocity magnitude under the conditions integrated with the weather prediction data. These profiles were sampled at five different locations (A, B, C, D, and E shown in 8(a)) at four different times (08:02:45, 08:02:55, 08:03:05, and 08:03:15). Locations D and E involve larger variations of wind velocity magnitude in the region $0\text{m} \leq z \leq 150\text{m}$ than the other locations. This is because locations D and E are included in the unsteady wake flow behind the hill as seen in Fig. 7. These results agree with the actual measurement by the Doppler radar; the study in [5] observed the wind speed with a variation of more than 20kt (10.3m/s) at the altitude above the runway (elevation = 27m) from 200ft (61.0m) to 400ft (121.9m).

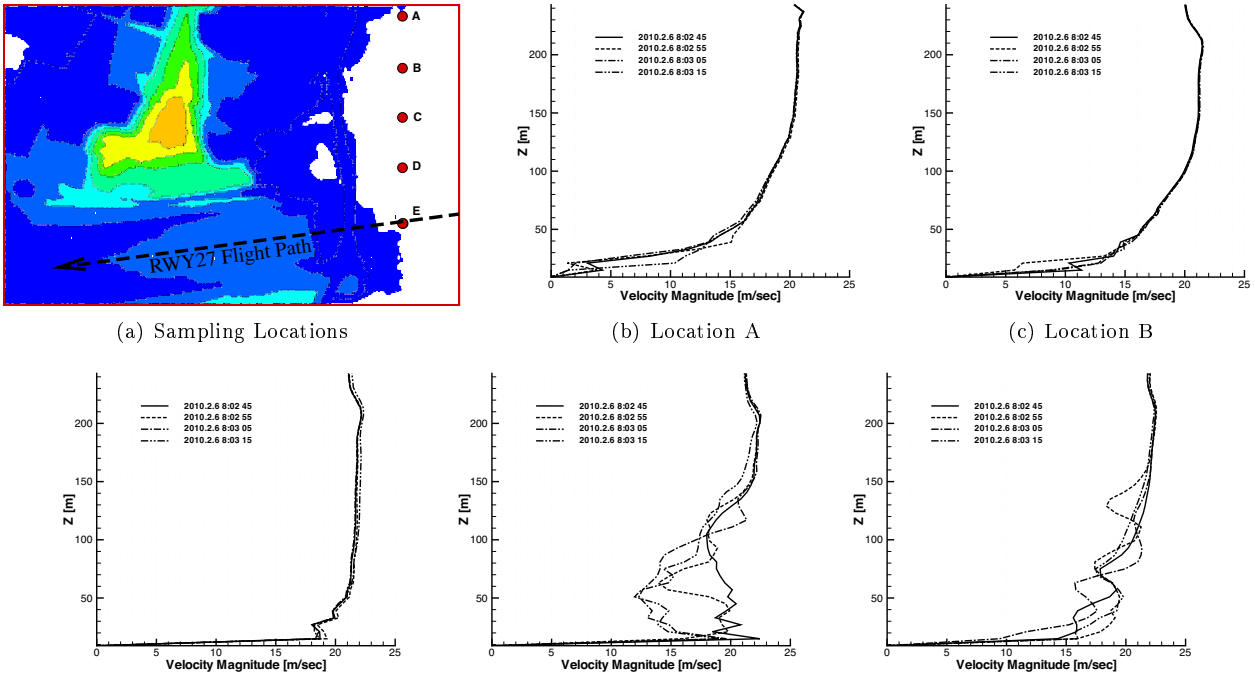

(a) Sampling Locations (b) Location A (c) Location B

(d) Location C (e) Location D (f) Location E

Figure 8: Vertical Profiles of Wind Velocity Magnitude Under the Conditions Integrated with Weather Prediction Data.

Figure 9 compares the contour plots of wind velocity magnitude simulated by the present LES with those observed by the Doppler radar (courtesy of Dr. Naoki Matayoshi and Dr. Masahiko Sugiura in the Aviation Program Group, JAXA). These plots are drawn on two different planes, which were scanned by the Doppler

radar with the elevation angle of 45deg and 75deg. The Doppler radar data contain missing values due to the interference with geographical features, which are plotted by white color. Open circles with black broken lines in Fig. 9 indicate the streaks of turbulence from the hill. The streaks appear at almost same locations in the present LES and the radar measurement, although one of the stream disappears due to data missing in the radar measurement. In addition, these streaks contain almost a same turbulence level; the present LES results in the maximum velocity magnitude of 26.1m/s while the radar measurement detects the maximum velocity magnitude of 30.4m/s. Therefore, the results in this section indicate that LES integrated with weather prediction data can simulate the turbulence induced by geographical features, and agree with actual turbulence qualitatively and quantitatively.

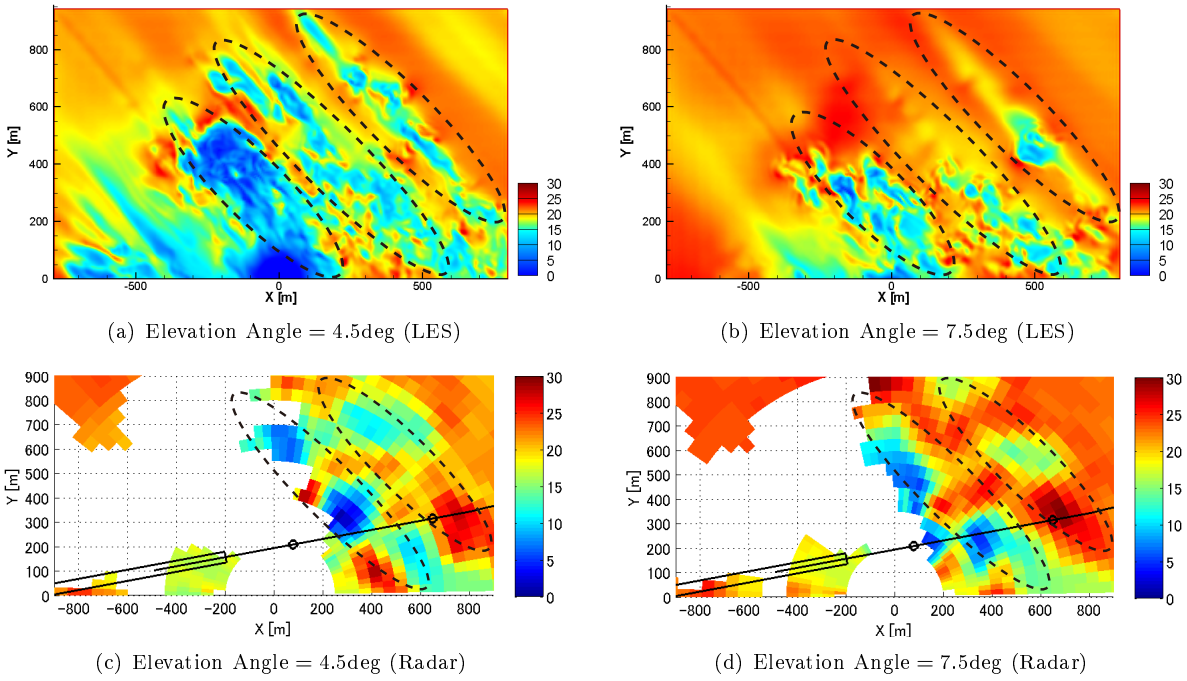

(a) Elevation Angle = 4.5deg (LES)

(b) Elevation Angle = 7.5deg (LES)

(c) Elevation Angle = 4.5deg (Radar)

(d) Elevation Angle = 7.5deg (Radar)

Figure 9: Contour Plots of Wind Velocity Magnitude [m/s].

5 Conclusions

This study implemented LES around Shonai Airport considering geographical features, and simulated the turbulence induced by a neighboring hill. This study employed the two-way nesting method to integrate LES with weather prediction by JMANHM, each which was implemented by solving difference governing equations in a difference zone with different scales. First, turbulence simulations were performed with uniform background flow conditions, and indicated that geographical features may have an significant influence on the turbulence appearing in flight path, i.e., aircraft safety depending on wind direction. Next, the turbulence simulation was integrated with the weather prediction data, and indicated that the present simulation can predict the turbulence induced by geographical features, and quite agree with the turbulence, which was actually observed by the Doppler radar.

Acknowledgment

The authors would like to appreciate Dr. Naoki Matayoshi and Dr. Masahiko Sugiura in the Aviation Program Group, JAXA for providing actual measurement data by the Doppler radar at Shonai Airport. In addition, this study implemented all simulations in a SGI UV 1000 supercomputer system owned by the Advanced

Fluid Information Research Center, Institute of Fluid Science, Tohoku University, Japan. The authors would also like to appreciate it for providing high-performance computer resources.

References

[1] Takeshi Ogasawara, Takashi Misaka, Toshihiro Ogawa, Shigeru Obayashi, and Izumi Yamada. Measurement of aircraft wake vortices using Doppler LIDAR. *Journal of Fluid Science and Technology*, 3(4):488–499, June 2008.

[2] Takashi Misaka, Takeshi Ogasawara, Shigeru Obayashi, Izumi Yamada, and Yoshinori Okuno. Assimilation experiment of lidar measurements for wake turbulence. *Journal of Fluid Science and Technology*, 3(4):512–518, June 2008.

[3] Hiroshi Kato. *Prediction of Wake Turbulence Behaviors Using Weather Observation and Simulation*. Master thesis, Tohoku University, Sendai, Japan, March 2010. (in Japanese).

[4] Kentaro Yamamoto. Observation of low-level wind shear without precipitation by Doppler LIDAR for airport weather. *Tenki*, 56(10):848–854, October 2009. (in Japanese).

[5] Naoki Matayoshi, Masahiko Sugiura, Eiichi Yoshikawa, Satoru Yoshida, Takeshi Morimoto, Tomoo Ushio, and Zenichiro Kawasaki. Low-level turbulence observation at Shonai airport. In *Proceedings of the 41st Japan Society for Aeronautical and Space Sciences Annual Meeting*, pages 576–583, April 2010. (in Japanese).

[6] Naoki Matayoshi, Masahiko Sugiura, Eiichi Yoshikawa, Tomoo Ushio, and Zenichiro Kawasaki. Development of low-level turbulence advisory system around airport. In *Proceedings of the 49th Aircraft Symposium*, pages 1061–1066, October 2011. (in Japanese).

[7] William C. Skamarock, Joseph B. Klemp, Jimy Dudhia, David O. Gill, Dale M. Barker, Wei Wang, and Jordan G. Powers. A description of the advanced research WRF version 2. Technical Report NCAR/TN–468+STR, Mesoscale and Microscale Meteorology Division, National Center for Atmospheric Research, Boulder, CO, June 2005.

[8] Kazuo Saito, Teruyuki Kato, Hisaki Eito, and Chiashi Muroi. Documentation of the Meteorological Research Institute / Numerical Prediction Division unified nonhydrostatic model. Technical Report 42, Meteorological Research Institute, Tsukuba, Japan, March 2001.

[9] GTOPO30 – Global 30 Arc Second Elevation Data Set. http://www1.gsi.go.jp/geowww/globalmap-gsi/gtopo30/gtopo30.html [cited 2 July 2012].

[10] Global Land Cover Characterization. http://edc2.usgs.gov/glcc/glcc.php [cited 2 July 2012].

[11] Geospatial Information Authority of Japan. http://www.gsi.go.jp/kiban/ (in Japanese) [cited 2 July 2012].

[12] Shaohua Shen, Feng Ding, Jongil Han, Yuh-Lang Lin, S. Pal Arya, and Fred H. Proctor. Numerical modeling studies of wake vortices: Real case simulations. In *37th AIAA Aerospace Sciences Meeting and Exhibit*, AIAA Paper 99–755, Reston, VA, January 1999. AIAA.

[13] Phillip L. Roe. Approximate Riemann solvers, parameter vectors, and difference schemes. *Journal of Computational Physics*, 43(2):357–372, October 1981.

[14] Bram van Leer. Towards the ultimate conservative difference scheme. V. a second-order sequel to Godunov's method. *Journal of Computational Physics*, 32(1):101–136, 1979.